

Compression phase is not necessary for generalization in representation learning

Sungyeop Lee^{1,*} and Junghyo Jo^{2,3,†}

¹*Department of Physics and Astronomy,*

Seoul National University, Seoul 08826, Korea

²*Department of Physics Education and Center for
Theoretical Physics and Artificial Intelligence Institute,*

Seoul National University, Seoul 08826, Korea

³*School of Computational Sciences, Korea Institute for Advanced Study, Seoul 02455, Korea*

(Dated: November 30, 2021)

Abstract

The outstanding performance of deep learning in various fields has been a fundamental query, which can be potentially examined using information theory that interprets the learning process as the transmission and compression of information. Information plane analyses of the mutual information between the input-hidden-output layers demonstrated two distinct learning phases of fitting and compression. It is debatable if the compression phase is necessary to generalize the input-output relations extracted from training data. In this study, we investigated this through experiments with various species of autoencoders and evaluated their information processing phase with an accurate kernel-based estimator of mutual information. Given sufficient training data, vanilla autoencoders demonstrated the compression phase, which was amplified after imposing sparsity regularization for hidden activities. However, we found that the compression phase is not universally observed in different species of autoencoders, including variational autoencoders, that have special constraints on network weights or manifold of hidden space. These types of autoencoders exhibited perfect generalization ability for test data without requiring the compression phase. Thus, we conclude that the compression phase is not necessary for generalization in representation learning.

* dtd2001@snu.ac.kr

† jojunghyo@snu.ac.kr

I. INTRODUCTION

Since the development of information theory as a theory of communication by Shannon [1, 2], it has played a crucial role in various domains of engineering and science, including physics [3], biology [4], and machine learning [5]. The information bottleneck (IB) theory interprets the learning process of neural networks as the transmission and compression of information [6]. Neural networks encode input X into their internal representation Z ; then, they decode Z to predict the desired output Y . The IB theory is a rate-distortion theory that compresses irrelevant information in X for predicting Y to the maximum extent. The objective function of this theory can be mathematically described as minimizing the mutual information $I(X; Z)$ between X and Z , given a required transmission of the mutual information $I(Z; Y)$ between Z and Y :

$$\min_{p(Z|X)} I(X; Z) - \beta I(Z; Y), \quad (1)$$

where β is a trade-off coefficient that balances the information compression and transmission.

The mutual information provides a potent tool for visualizing the learning processes by displaying a trajectory on the two-dimensional plane of $I(X; Z)$ and $I(Z; Y)$, called the *information plane* (IP). Through IP analyses, Shwartz-Ziv and Tishby found that the training dynamics of neural networks demonstrates a transition between two distinct phases: fitting and compression [7, 8]. Supervised learning experiences a short fitting phase in which the training error is significantly reduced. This first phase is characterized by the increase in both $I(X; Z)$ and $I(Z; Y)$. Then, in the learning process, a large amount of time is spent on finding the efficient internal representation Z of input X when the fitting phase secures a small training error. During this second phase of compression, $I(X; Z)$ decreases while $I(Z; Y)$ remains constant. The compression phase has been argued to be associated with the generalization ability of machine learning by compressing irrelevant information of training data to prevent overfitting [8]. The non-trivial compression phase and its association to generalization have been further observed in other studies using different network models with different data; however, the universality of the compression phase remains debatable [9–11].

The debates can be partly attributed to the sensitivity toward the architecture of neural networks, activation functions, and estimation schemes of information measures. In this study, we investigated the universality of the compression phase using autoencoders (AEs) and robust kernel-based estimation of mutual information. AEs are neural networks that encode input X into internal representation Z and reproduce X by decoding Z . This representation learning can be interpreted as

self supervised learning where a label is input as itself, such as $Y = X$. To examine the IP analyses of representation learning, we considered AEs because (i) they have a concrete guide ($Y = X$) for checking the validity of $I(X; Z)$ and $I(Z; Y)$ on the IP; (ii) they have various species to explore trajectories on the IP; and (iii) they are closely related to unsupervised learning.

The remainder of this paper is organized as follows. We introduce various types of AEs in Section II and explain our kernel-based method for estimating mutual information in Section III. Then, we examine the IP trajectories of information transmission and compression of the AEs in Section IV. Finally, we summarize and discuss our findings in Section V.

II. REPRESENTATION LEARNING IN AUTOENCODERS

A. Information plane of autoencoders

AEs are neural networks specialized for dimensional reduction and representation learning in unsupervised manner. A deep AE consists of a symmetric structure with encoders and decoders as follows:

$$X - E_1 - \cdots - E_L - Z - D_1 - \cdots - D_L - X'. \quad (2)$$

where E_i and D_i denote the i -th encoder and decoder layer, respectively, and Z is the bottleneck representation with the smallest dimension. The deep AE trains an identity function to reproduce input X from output X' . During the training process, the AE extracts relevant features for reproducing X while compressing the high-dimensional input X into an internal representation Z on a low-dimensional bottleneck layer. The encoder and decoder layers form Markov chains that should satisfy the *data processing inequality* (DPI), analogous to supervised learning [12]:

$$\text{Forward DPI:} \quad I(X; E_1) \geq \cdots \geq I(X; E_L) \geq I(X; Z), \quad (3)$$

$$\text{Backward DPI:} \quad I(Z; X') \leq I(D_1; X') \leq \cdots \leq I(D_L; X'). \quad (4)$$

The forward DPI represents information compression as input X is processed into the bottleneck layer, whereas the backward DPI represents information expansion as the compressed representation Z is transformed into output X' .

The desired output of this AE is identical to the input ($X' = X$). This identity constrains the input and output mutual information to be located on a straight line $I(X; T) = I(T; X)$ for arbitrary internal representations, $T \in \{E_1, \dots, E_L, Z, D_1, \dots, D_L\}$. Here, if the desired output

X in $I(T; X)$ is replaced with the predicted output X' of the AE, the learning dynamics of the AE on the IP can be analyzed [12]. Then, the two sets of mutual information for representing information compression and transmission correspond to

$$I(X; T) = H(T) - H(T|X) \quad (5)$$

$$I(T; X') = H(T) - H(T|X'), \quad (6)$$

where $H(T)$ represents the Shannon entropy of T , and $H(T|X)$ and $H(T|X')$ are the conditional entropies of T given X and X' , respectively. The forward process of the AE realizes the deterministic mapping of $T = T(X)$ and $X' = X'(T)$. Then, one-to-one correspondence of $X \rightarrow T$ implies no uncertainty for $H(T(X)|X) = 0$, whereas possibly many-to-one correspondence of $T \rightarrow X'$ implies some uncertainty for $H(T|X'(T)) \neq 0$. Therefore, the inequality of $I(X; T) \geq I(T; X')$ is evident because $H(T) \geq H(T) - H(T|X')$, where the conditional entropy $H(T|X')$ is non-negative. Based on this inequality, the learning trajectory of $I(X; T)$ and $I(T; X')$ on the two-dimensional IP (x, y) can be expected to stay below the diagonal line $y = x$. Once the learning process of the AE is complete with $X' = X$, the two sets of mutual information become equal to $I(X; T) = I(T; X' = X)$, and the learning trajectory ends up on the diagonal line.

B. Various types of autoencoders

Because the existence of the compression phase is an empirical observation rather than an analytical result, it is unclear whether this non-trivial phase is necessary for the generalization of representation learning. To investigate this, we adopted AEs because their theoretical bound of IP trajectories can guide our IP analysis. IP analysis has been used to visualize the information process in AEs [12, 13]. Their IP trajectories satisfied the theoretical bound of $I(X; T) \geq I(T; X')$. Previous studies examined IP trajectories according to the size of the bottleneck layer, but they did not investigate the association between the compression phase and generalization of AEs. Another important advantage of adopting AEs is their diverse variants that enable us to fully explore IP trajectories. In particular, because a certain AE model is directly linked to unsupervised learning, the model can be used to understand the information process of unsupervised learning. Now, we briefly introduce diverse species of AEs used in our experiments.

The simplest structure of AE, called shallow AE, consists of a single bottleneck layer between the input and output layers. In the shallow AE ($X - Z - X'$), the forward propagation of input X

is defined as

$$Z = f_E(W_E X + b_E) \quad (7)$$

$$X' = f_D(W_D Z + b_D), \quad (8)$$

where W and b represent the weights and biases, respectively, and $f(s)$ is a corresponding activation function. Here, the subscripts E and D denote encoder and decoder, respectively. The shallow AE is trained to minimize the reconstruction errors usually measured by the mean squared error (MSE) between output X' and desired output X . It has been analytically proved that a shallow AE with linear activation ($f(s) = s$) spans the same subspace as that spanned by principal component analysis (PCA) [14, 15]. Deep AEs stack hidden layers in the encoder and decoder symmetrically; moreover, it is well known that deep AEs yield better compression than shallow AEs.

Until recently, a myriad of variants and techniques have been proposed to improve the performance of AEs via richer representations, such as sparse AE (SAE) [16], tied AE (TAE) [17], variational AE (VAE) [18], and label AE (LAE)[19, 20].

- SAE was proposed to avoid overfitting by imposing sparsity in the latent space. The sparsity penalty is considered a regularization term of the Kullback-Leibler (KL) divergence between the activity of bottleneck layer Z and sparsity parameter ρ , a small value close to zero.
- TAE shares the weights for the encoder and decoder part ($W_E = W_D^T$), where superscript T depicts the transpose of a matrix. This model is widely used to reduce the number of model parameters while maintaining the training performance. Owing to its symmetrical structure, it can be interpreted as a deterministic version of restricted Boltzmann machines (RBMs), a representative generative model for unsupervised learning; consequently, the duality between TAE and RBM has been identified [21]. Compared to the vanilla AE, SAE and TAE have regularization in the degrees of freedom for nodes and weights, respectively. Later, we visually validate how these constraints lead to a difference in the information flow of IP trajectories.
- The ultimate goal of AEs is to obtain richer expressions in the latent space. Therefore, an AE is not a mere replica model, but a generative model that designs a tangible latent representation to faithfully reproduce the input data as output. VAE is one of the most representative generative model with a similar network structure as AE; however, its mathematical formulation is fundamentally different. The detailed derivation of the learning algorithm of

VAE is beyond the scope of this study, and thus will be omitted [18]. In brief, the encoder network of VAE realizes an approximate posterior distribution $q_\phi(Z|X)$ for variational inference, while the decoder network realizes a distribution $p_\theta(X|Z)$ for generation. The loss of VAE, known as the evidence lower bound (ELBO), is decomposed into a reconstruction error given by the binary cross entropy (BCE) between the desired output X and predicted output X' , and the regularization of KL divergence between the approximate posterior distribution $q_\phi(Z|X)$ and prior distribution $p(Z)$. Because tangible Gaussian distributions are usually adopted as the approximate posterior and prior distributions of $q_\phi(Z|X)$ and $p(Z)$, respectively, VAE has a special manifold of the latent variable Z .

- AEs do not use data labels. Instead, inputs work as self labels for supervised learning. Here, to design the latent space using label guides, we consider another AE, called Label AE (LAE). LAE enforces the input data to be mapped into the latent space with their corresponding label classification. Then, the label-based internal representation is decoded to reproduce input data. Although the concept of regularization using labels has been proposed [19, 20], LAE has not been considered as a generative model. Unlike vanilla AEs that use a sigmoid activation function, LAE uses a softmax activation function, $f(Z_i) = (\exp Z_i) / (\sum_j \exp Z_j)$, to impose the regularization of the internal representation Z to follow the true label Y as the cross entropy (CE) between Y and Z . Once LAE is trained, it can generate learned data or images using its decoder, starting from one hot vector Z of labels with the addition of noise. Additional details of LAE are provided in appendix B. Later, we compare the IP trajectories of VAE and LAE with those of vanilla AE in deep structure to examine how the information flow varies depending on the latent space of generative models.

Table 1 summarizes the loss function, constraints, and activation function of the bottleneck layer for each aforementioned AE model.

III. ESTIMATION OF MUTUAL INFORMATION

After preparing various species of AE models to explore diverse learning paths on the IP, we accurately estimate the mutual information for IP analyses:

$$I(X; Z) = \sum_{x,z} p(x, z) \log \frac{p(x, z)}{p(x)p(z)}. \quad (9)$$

Model	Main Loss	Constraint	Bottleneck activation
AE	$\text{MSE}(X, X')$	None	sigmoid
SAE	$\text{MSE}(X, X')$	$\text{KL}(\rho Z)$	sigmoid
TAE	$\text{MSE}(X, X')$	$W_E = W_D^T$	sigmoid
VAE	$\text{BCE}(X, X')$	$\text{KL}(q_\phi(Z X) p(Z))$	Gaussian sampling
LAE	$\text{MSE}(X, X')$	$\text{CE}(Y, Z)$	softmax

TABLE I. Various species of autoencoders. Vanilla AE uses the mean squared error (MSE) loss. We used a sigmoid function as an activation function for the bottleneck layer, which helps in unifying the scales of different layers. Regularization of SAE is the KL-divergence between the hidden activity and sparsity parameter ρ . The only difference in TAE is that it shares the weight of encoder and decoder. The loss function of VAE, known as the evidence lower bound (ELBO), consists of the reconstruction error, binary cross entropy (BCE), and KL-divergence between the approximate posterior $q_\phi(Z|X)$ and prior $p(Z)$; moreover, the stochastic node activities of the bottleneck layer are sampled from Gaussian distributions. In LAE, the classification error, cross entropy (CE) between the softmax hidden activity Z and true label Y , is used as a regularization term.

In reality, we have samples of data, $\{x(t), z(t)\}_{t=1}^N$, instead of their probabilities, $p(x)$, $p(z)$, and $p(x, z)$. Using N samples of data, we may estimate the probabilities. Here, if X and Z are continuous variables, it is inevitable to first discretize them. Then, we can count the discretized samples for each bin and estimate the probabilities. The estimation of mutual information based on this binning method has some limitations. First, its accuracy depends on the resolution of discretization. Second, large samples are required to properly estimate the probability distributions. Suppose that X is an n -dimensional vector. Despite considering the most naive discretization, the total number of configurations for binarized X is already 2^n . Therefore, other schemes such as kernel density estimation [22], k-nearest neighbor, and kernel-based estimators [23] exist to estimate the entropy and mutual information. The description of each scheme and corresponding IP results are summarized in a pedagogical review [24]. Among these various methods, we adopted a kernel-based estimator, which is mathematically well defined and computationally efficient for large networks. It estimates the Renyi α -entropy using the eigenspectrum of covariance matrix of X as follows:

$$S_\alpha(A) = \frac{1}{1-\alpha} \log_2 [\text{tr}(A^\alpha)] = \frac{1}{1-\alpha} \log_2 \left[\sum_{i=1}^N \lambda_i(A)^\alpha \right], \quad (10)$$

where A is an $N \times N$ normalized Gram matrix of random variable X with size N and $\lambda_i(A)$ is the i -th eigenvalue of A . Note that tr denotes the trace of a matrix. In the limit of $\alpha \rightarrow 1$, Eq. (10) is reduced to the familiar Shannon entropy of $H(X)$. If we assume that B is a normalized Gram matrix from another random variable Y , the joint entropy between X and Y is defined as

$$S_\alpha(A, B) = S_\alpha \left(\frac{A \circ B}{\text{tr}(A \circ B)} \right), \quad (11)$$

where $A \circ B$ denotes the Hadamard product, i.e., the element-wise product of two matrices. From equations (10) and (11), the mutual information can be defined as

$$I_\alpha(A, B) = S_\alpha(A) + S_\alpha(B) - S_\alpha(A, B). \quad (12)$$

Using this kernel-based estimator, Yu and Principe visualized the IP trajectories of AEs and suggested the optimal design of AEs based on IP patterns [12]. The kernel-based estimator contains a hyperparameter that defines a kernel function of distances between samples. Because the estimator depends on the dimension and scale of variables for samples, the hyperparameter should be carefully determined [13]. Despite careful determination, the kernel-based estimator seems unstable because it is sensitive to the training setup of neural networks. Moreover, once the information process of deep neural networks is quantified by this estimator, it sometimes violates the DPI, which is a necessary condition for interpreting layer stacks as Markov chains.

We found that the raw activities of neural networks can result in inaccurate entropy estimation irrespective of the estimation schemes when they have different dimensions and scales depending on layers. Large activities tend to overestimate their entropy, whereas low activities tend to underestimate their entropy. In particular, the use of linear activation function or Rectified Linear Unit (ReLU) often results in the violation of DPI. To address this issue, we unified to use a bounded activation function, i.e., sigmoid function ($f(s) = 1/(1 + \exp(-s))$), except for VAE and LAE whose bottleneck layers use Gaussian sampling and softmax function, respectively and this setup eliminated DPI violation. Saxe *et al.* argued that using double-sided saturating activation functions such as $f(s) = \tanh(s)$ trivially induces the compression phase on the IP, and it is not related to the generalization of machine learning [9]. They showed that the mutual information, estimated by the binning method, first increases and then decreases as the weight parameters of neural networks get larger. The second decreasing phase of mutual information causes the compression phase. We performed the same task with various activation functions, including sigmoid and ReLU, but we estimated the mutual information using the aforementioned kernel-based method. Then, we confirmed that the second decreasing phase did not occur by merely increasing the weight parameters,

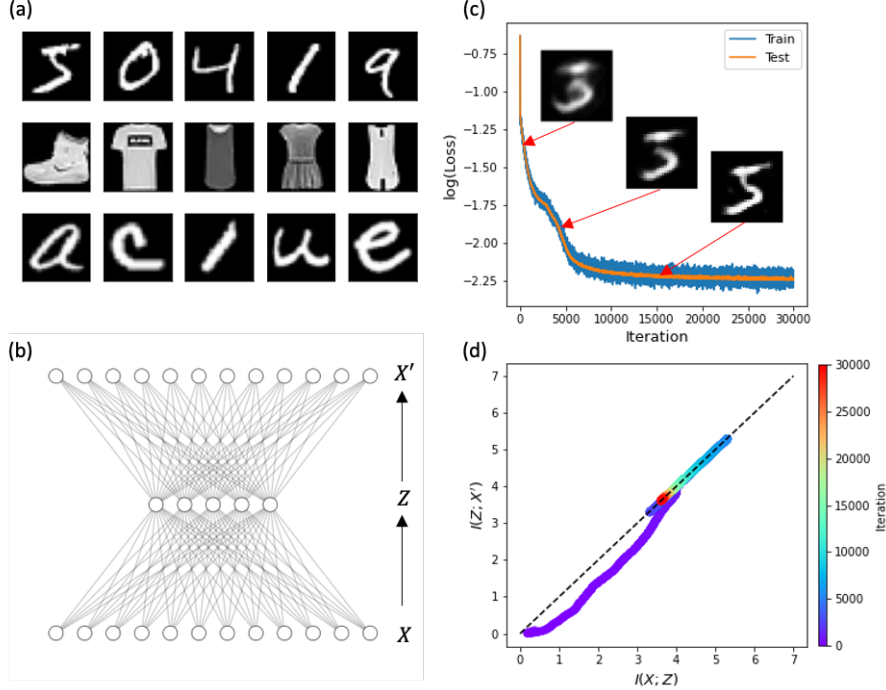


FIG. 1. Information transmission and compression of autoencoders. (a) Image datasets X of MNIST (top row), Fashion-MNIST (middle), and EMNIST (bottom). (b) Network structure of a shallow autoencoder: input X , hidden Z , and output X' . Note that node numbers are arbitrary for a schematic display. (c) Error (or loss) between desired output X and reconstructed output X' for training (blue) and test (orange) data during learning iterations. Insets are snapshots of reconstructed X' at some iterations. (d) Trajectory of mutual information ($I(X; Z)$, $I(Z; X')$) on the information plane. Color bar represents the number of iterations.

suggesting that the IP paths do not depend on the selection of activation functions in our kernel-based method. Further details on this experiment are provided in Appendix A. For those who are interested in using IP analysis, we have provided the complete source code and documentation on GitHub [25].

IV. RESULTS

A. Compression phase of autoencoders

After the robust kernel-based estimation of mutual information, we examined the IP trajectories of various species of AEs. In this study, we investigated the information process of representation

learning for real image datasets (figure 1(a)): MNIST [26], Fashion-MNIST [27], and EMNIST [28]. MNIST has 60,000 training and 10,000 testing images of 28×28 pixels of 10 hand-written digits (0-9). Fashion-MNIST has the same data size as MNIST for 10 different fashion products such as dresses or shirts. Finally, EMNIST is an extension of MNIST; it contains 10 digits and 26 uppercase (A-Z) and lowercase letters (a-z). In this paper, we focused on the results of MNIST because the results of Fashion-MNIST and EMNIST are basically the same (refer [25]).

For representation learning of MNIST, we first considered a shallow AE ($X - Z - X'$) that includes a single hidden or bottleneck layer (figure 1(b)). The input, hidden, and output layers have $n_X = 28 \times 28 = 784$, $n_Z = 50$, and $n_{X'} = 784$ nodes, respectively. We considered a fully-connected network between layers with the loss functions listed in Table I. For the optimization of network weights, we used the stochastic gradient descent method with Adam optimization, given a batch size of 100 for a total of 50 epochs. With each learning iteration, the $\text{MSE}(X, X')$ keeps decreasing (figure 1(c)). This implies that the output X' of AE successfully reproduces the input image X of training data. To measure the generalization ability of the AE, we examined the reproduction ability of the AE for test images that were not used in the learning process. Accordingly, we confirmed that the test error is as small as the training error, suggesting perfect generalization of shallow AE. The IP trajectory of the AE during the learning process is presented in figure 1(d). As expected, the trajectory satisfies the inequality of $I(X; Z) \geq I(Z; X')$, and ends up on their equality line because of $X' \approx X$ at the end of training. As observed by Shwartz and Ziv [8], the IP trajectory shows two distinct phases of fitting and compression. In the initial fitting phase, the input mutual information $I(X; Z)$ between X and Z increases. Then, during the second compression phase, $I(X; Z)$ decreases. Note that this representation learning shows a simultaneous decrease in the output mutual information $I(Z; Y = X')$, whereas general supervised learning maintains $I(Z; Y)$ to be constant during the compression phase.

Next, we considered a deep AE ($X - E_1 - E_2 - Z - D_1 - D_2 - X'$) with two additional encoder layers before the bottleneck layer and two decoder layers after the bottleneck layer (figure 2(a)). The corresponding node numbers for the inner layers are $n_{E_1} = 256$, $n_{E_2} = 128$, $n_Z = 50$, $n_{D_1} = 128$, and $n_{D_2} = 256$. The deep AE exhibited similar learning accuracy and generalization ability as the shallow AE (figure 2(b)). During the learning process, we measured the mutual information using the kernel-based estimator and confirmed that the learning process of the deep AE satisfied the DPI (figure 2(c)). We observed the compression phase in the inner layers of E_2 , Z , and D_1 (figure 2(d)). However, the compression phase was not evident in the outer layers of E_1 and D_2 .

that have relatively large dimensions with high information capacity.

Subsequently, we explore whether the compression phase appears even with a small amount of training data. Unless sufficient training data are provided, machine learning can easily overfit the small amount of training data and fail to generalize the test data. We conducted a learning experiment with the deep AE using 10% of the total training data. The training error kept decreasing, similar to the training error given the full training data. However, the test error is significantly larger than the training error (figure 2(e)). This demonstrates that the deep AE fails to generalize. After confirming the satisfaction of DPI (figure 2(f)), we examined the IP trajectories. Unlike the results of full training data, we did not observe the compression phase from any layers (figure 2(g)). Thus, this difference suggests that the compression phase seems to be associated with generalization.

B. Sparse activity and constrained weights

To further analyze the compression phase, we considered different species of AEs that can modify the compression process of learning. SAE and TAE have additional regularization for node activities and weight parameters, respectively, in comparison to vanilla AE (Table 1). First, we examined SAE that has the same structure as shallow AE. SAE shows perfect learning and generalization (figure 3(a)). It is of particular interest that the compression phase is markedly exaggerated in SAE (figure 3(b)). The sparsity penalty of SAE turns off unnecessary activities of hidden nodes, which can accelerate the compression phase.

Second, we examined TAE that also has the same structure as shallow AE and SAE, but has a weight constraint of $W_E = W_D^T$. Similar to shallow AE and SAE, TAE shows perfect learning and generalization; however, its learning accuracy is slightly lower under the weight constraint (figure 3(c)). However, TAE did not exhibit the compression phase (figure 3(d)). This implies that the compression phase is not necessary for generalization. Given the weight constraint, TAE seems to have less potential capacity to remove irrelevant information than vanilla AE.

C. Constrained latent space

We obtained a clear counterexample of TAE demonstrating that the compression phase is not necessary for generalization. Now, we survey another species of AEs that more actively modify

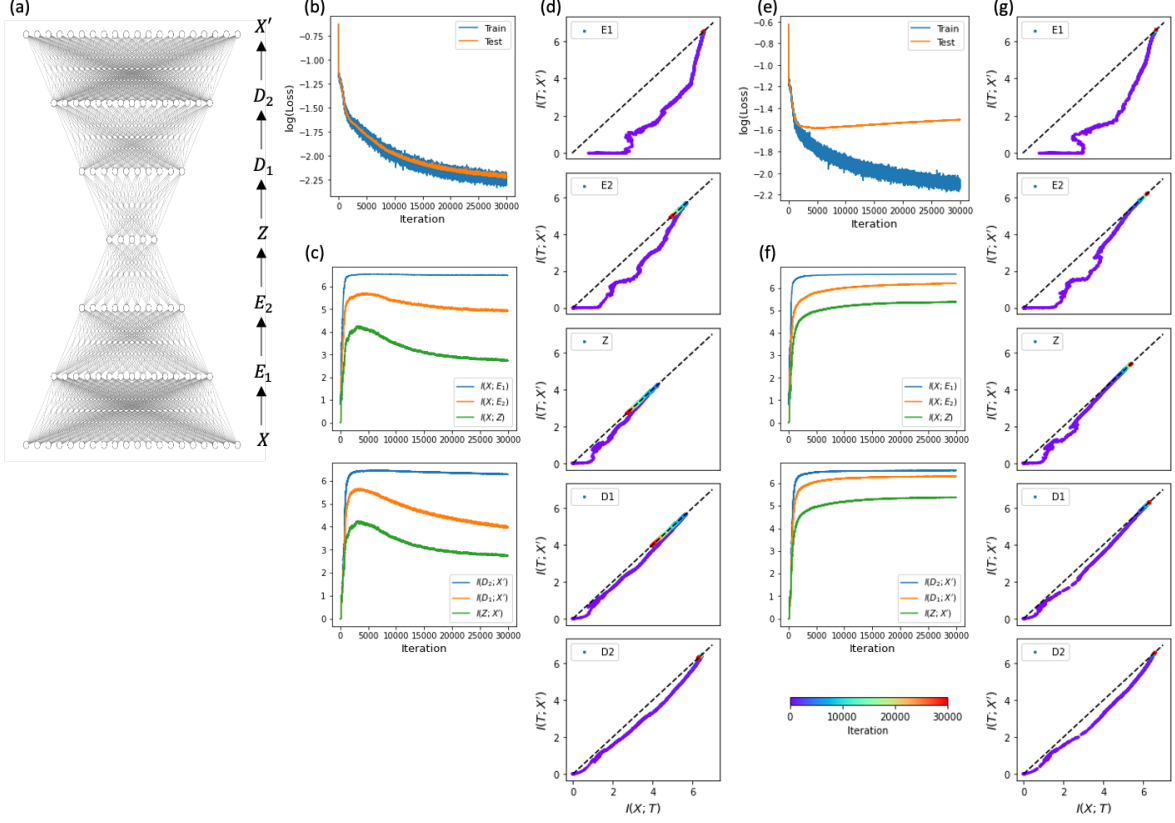


FIG. 2. Compression phase and generalization of representation learning. (a) A deep autoencoder with input X , two encoders, E_1 and E_2 , bottleneck Z , two decoders, D_1 and D_2 , and output X' . (b) Learning errors for training (blue) and test (orange) data during iterations. (c) Changes in input mutual information (upper) and output mutual information (lower) during iterations. (d) Learning trajectories on the information plane. The general variable T stands for E_1 , E_2 , Z , D_1 , or, D_2 . (b-d) Experiments with full training set of 60,000 MNIST data. (e-g) Experiments with 10% training set of 6,000 MNIST data.

the latent space of the bottleneck layer, and further investigate the existence of the compression phase for generalization.

VAE is a generative model that maps input data X into a Gaussian distribution $q_\phi(Z|X)$ for the latent variable Z . We considered a deep VAE that has the same structure ($X - E_1 - E_2 - Z - D_1 - D_2 - X'$) as deep AE, and confirmed that the VAE can learn the training data of MNIST and generalize to reproduce the test data (figure 4(a)). However, because VAE has a special constraint for the bottleneck layer, the information process from the input layer into the bottleneck layer does not satisfy the DPI (figure 4(b)). The mutual information $I(X; Z)$ between X and Z does not change during the training process. Indeed, the fixed value is close to the maximum entropy

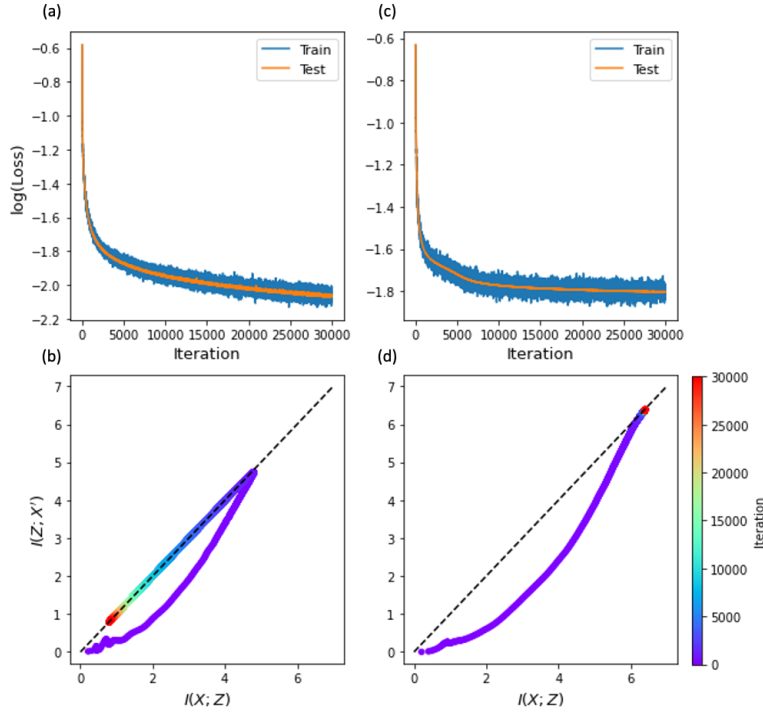


FIG. 3. Information compression in constrained autoencoders. (a) Learning errors for training (blue) and test (orange) data during iterations. (b) Learning trajectories on the information plane. (a,b) Results of sparse autoencoders (SAE). (c,d) Results of tied autoencoders (TAE). The network structure of SAE and TAE can be represented by $X - Z - X'$.

of X given its batch size of 100 samples, $I(X; Z) \approx \log_2(100) \approx 6.6$, which is independent on dimension n_Z of Z (data not shown). It is noteworthy that the mutual information between X and Z does not change for the learning process, although the mapping $X \rightarrow Z$ keeps reorganizing to distinguish the feature difference of X . This shows a limitation of the information measure $I(X; Z)$ that fails to capture the content-dependent representation of Z . Except for the bottleneck layer, other layers still satisfy the DPI. Next, we displayed the IP trajectories of VAE for each layer (figure 4(c)). We did not observe the compression phase in any layer in the VAE. Therefore, VAE can generalize without the compression phase, similar to TAE.

LAE is another generative model that maps X into Z , where Z corresponds to label Y of X . Thus, unlike other AE models, LAE uses label information to shape its latent space. We used the same deep network structure like the deep AE and VAE for LAE. The deep LAE can also learn the training data of MNIST and generalize to reproduce the test data as well (figure 4(d)). LAE satisfies the DPI (figure 4(e)) and its IP trajectories also satisfy the inequality of $I(X; T) \geq I(T; X')$

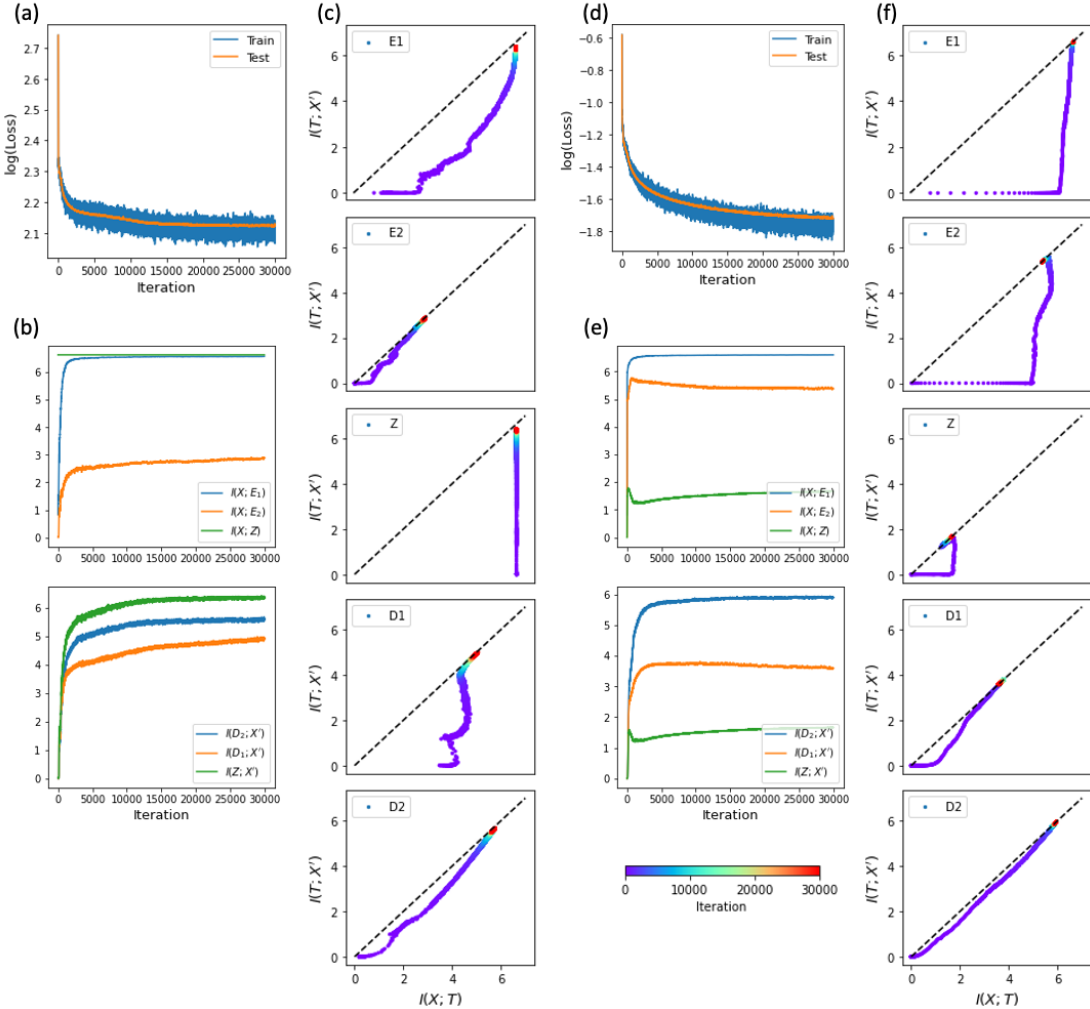


FIG. 4. Information trajectories of generative models. (a) Learning errors for training (blue) and test (orange) data during iterations. (b) Changes in the input mutual information (upper) and output mutual information (lower) during iterations. (c) Learning trajectories on the information plane. (a-c) Results of a variational autoencoder (VAE). (d-f) Results of a label autoencoder (LAE). VAE and LAE have a deep network structure with $X - E_1 - E_2 - Z - D_1 - D_2 - X'$. The general variable T denotes for E_1, E_2, Z, D_1 , or D_2 .

(figure 4(f)). It is interesting that LAE has orthogonal learning phases. LAE first increases the input mutual information $I(X; T)$ for the encoding part. Once LAE arrives at a certain maximal $I(X; T)$, the output mutual information $I(T; X')$ starts to increase. This shows that LAE first extracts information from the input data relevant for their label classification, and then transfers information to output for reproducing input images. We found that the LAE did not exhibit the

compression phase even though it successfully generalized.

V. DISCUSSIONS

In summary, we studied the information flows in the internal representations of AEs using a robust kernel-based estimator of mutual information. When we used sufficient training data, shallow and deep AEs demonstrated the compression phase, following the fitting phase, along with the generalization ability to reproduce test data, thereby confirming the original proposal by Shwartz-Ziv and Tishby [8]. However, when we used a small amount of training data to induce overfitting, the AEs did not exhibit compression phase and generalization, suggesting that the compression phase is associated with generalization. When a sparsity constraint was imposed in the hidden activities of SAE, regularization amplified the compression phase and provided more efficient representations for generalization. However, the constraining weight parameters ($W_E = W_D^T$) of TAE showed perfect generalization in the absence of the compression phase. Furthermore, VAE and LAE, shaping the latent space with a variational distribution and label information, also achieved generalization without the compression phase. These counterexamples of TAE, VAE, and LAE clearly demonstrate that the compression phase is not necessary for the generalization of models.

It is noteworthy that the absence of the compression phase does not mean that compression does not occur in representation learning. When the encoder part has a narrowing architecture, information compression is inevitable, as demonstrated by the DPI. Then, the removal of irrelevant information from data may contribute to the generalization of models. After the completion of representation learning, AEs obtain a certain amount of mutual information $I(X; Z) = I_f$ between the input data X and its internal representation Z . The paths that obtain I_f seem different between AEs. In TAE, VAE, and LAE, $I(X; Z)$ monotonically increases to I_f . However, in vanilla AE and SAE, $I(X; Z)$ first increases beyond I_f , and then decreases back to I_f . The backward process is called the compression phase. Because the loss function of representation learning never includes any instruction for the path of $I(X; Z)$, it is not surprising that the existence of the compression phase is not universal.

Observing and controlling the information flow in neural networks is crucial for understanding and designing a better deep learning algorithm. IP analysis is an excellent tool to monitor information transmission and compression inside the “black box” of neural networks. For IP analysis, accurate information estimation is a prerequisite. We used kernel-based estimation for comput-

tational efficiency. Accordingly, we found that it is critical to use bounded activation functions. When we used ReLU as an activation function, the DPI was easily violated, although we observed the compression phase in this setting. Thus, it can be problematic to estimate the mutual information from unbounded variables with different scales for different layers. In this study, we provided a concrete ground to further explore the theoretical understanding for information processing in deep learning.

ACKNOWLEDGEMENT

This work is supported in part by the National Research Foundation of Korea (NRF) grant (Grant No. 2018R1A2B6004914) (S.L.), the New Faculty Startup Fund from Seoul National University, and the NRF grant funded by the Korea government (MSIT) (Grant No. 2019R1F1A1052916) (J.J.).

- [1] Claude E Shannon. A mathematical theory of communication. *The bell system technical journal*, 27(3):379–423, 1948.
- [2] Thomas M Cover. *Elements of information theory*. John Wiley & Sons, 1999.
- [3] Edwin T Jaynes. Information theory and statistical mechanics. *Physical review*, 106(4):620, 1957.
- [4] Hubert P Yockey. *Information theory, evolution, and the origin of life*. Cambridge University Press, 2005.
- [5] David JC MacKay and David JC Mac Kay. *Information theory, inference and learning algorithms*. Cambridge university press, 2003.
- [6] Naftali Tishby, Fernando C Pereira, and William Bialek. The information bottleneck method. *arXiv preprint physics/0004057*, 2000.
- [7] Naftali Tishby and Noga Zaslavsky. Deep learning and information bottleneck principle. *IEEE Information Theory Workshowp (ITX)*, pages 1–5, 2015.
- [8] Ravid Shwartz-Ziv and Naftali Tishby. Opening the black box of deep neural networks via information. *arXiv:1703.00810*, 2017.
- [9] Andrew M. Saxe, Yamini Bansal, Joel Dapello, Madhu Advani, Artemy Kolchinsky, Brendan D. Tracey, and David D. Cox. On the information bottleneck theory of deep learning. *Journal of Statistics*

tical Mechanics, 124020, 2019.

- [10] Ivan Chelombiev, Conor Houghton, and Cian O’Donnell. Adaptive estimators show information compression in deep neural networks. *arXiv:1902.09037*, 2019.
- [11] Kristoffer. Wickstrøm, Sigurd. Løkse, Michael. Kampffmeyer, Shujian. Yu, Jose. Principe, and Robert. Jenssen. Information plane analysis of deep neural networks via matrix-based Renyi’s entropy and tensor kernels. *arXiv:1909.11396*, 2019.
- [12] Shujian Yu and Jose C. Principe. Understanding autoencoders with information theoretic concepts. *Neural Networks*, 117:104–123, 2019.
- [13] Nicolás I. Tapia and Pablo A. Estévez. On the Information Plane of autoencoders. *International Joint Conference on Neural Networks*, 2020.
- [14] Hervé Bourlard and Yves Kamp. Auto-association by multilayer perceptrons and singular value decomposition. *Biological cybernetics*, 59.4:291–294, 1988.
- [15] Pierre Baldi and Kurt Hornik. Neural networks and principal component analysis: learning from examples without local minima. *Neural networks*, 2.1:53–58, 1989.
- [16] Andrew Ng. Sparse autoencoder. *CS294A Lecture notes*, 2011.
- [17] Pascal Vincent, Hugo Larochelle, Isabelle Lajoie, Yoshua Bengio, and Pierre-Antoine Manzagol. Stacked denoising autoencoders: learning a useful representations in a deep network with a local denoising criterion. *Journal of machine learning research*, 11.12, 2010.
- [18] Diederik P. Kingma and Max Welling. Auto-encoding variational bayes. *arXiv:1312.6114*, 2013.
- [19] Elyor Kodirov, Tao Xiang, and Shaogang Gong. Semantic autoencoder for zero-shot learning. *Proceedings of the IEEE conference on computer vision and pattern recognition*, pages 3174–3183, 2017.
- [20] Lei Le, Andrew Patterson, and Martha White. Supervised autoencoders: Improving generalization performance with unsupervised regularizers. *Advances in neural information processing systems*, 31:107–117, 2018.
- [21] Hanna Kamyshanska and Roland Memisevic. The potential energy of an autoencoder. *IEEE transactions on pattern analysis and machine intelligence*, 37.6:1261–1273, 2014.
- [22] Artemy Kolchinsky and Brenda D. Tracey. Estimating mixture entropy with pairwise distances. *Entropy*, 19.7:361, 2017.
- [23] Luis Gonzalo Sanchez Giraldo, Murali Rao, and Jose C. Principe. Measures of entropy form data using infinitely divisible kernels. *IEEE Transactions on Information Theory*, 61.1:535–548, 2014.

- [24] Bernhard C. Geiger. On information plane analyses of neural network classifiers - a review. *arXiv:2003.09671*, 2020.
- [25] Sungyeop Lee and Junghyo Jo. <https://github.com/Sungyeop/IPRL>, 2021.
- [26] Yann LeCun, Leon Bottou, Yoshua Bengio, and Patrick Haffner. Gradient-based learning applied to document recognition. *Proceedings of the IEEE*, pages 2278–2324, 1998.
- [27] Han Xiao, Kashif Rasul, and Roland Vollgraf. Fashion-mnist: a novel image dataset for benchmarking machine learning algorithms. *arXiv:1708.07747*, 2017.
- [28] Gregory Cohen, Saeed Afshar, Jonathan Tapson, and Andre Van Schaik. Emnist: Extending mnist to handwritten letters. In *2017 International Joint Conference on Neural Networks (IJCNN)*, pages 2921–2926. IEEE, 2017.
- [29] David W Scott. *Multivariate density estimation: theory, practice, and visualization*. John Wiley & Sons, 2015.
- [30] Bernard W. Silverman. *Density estimation for statistics and data analysis*. 26. CRC press, 1986.

Appendix A: Kernel-based mutual information estimator

The kernel-based method [23] estimates the Renyi α -entropy for a random variable X by

$$H_\alpha(X) = \frac{1}{1-\alpha} \int_{x \in \mathcal{X}} f_X^\alpha(x) dx. \quad (\text{A1})$$

In the limit of $\alpha \rightarrow 1$, equation (A1) is reduced to the Shannon entropy. Let $X = \{x_1, x_2, \dots, x_N\}$ denote N data points and $\kappa : \mathcal{X} \times \mathcal{X} \rightarrow \mathbb{R}$ be a real valued positive definite kernel that defines a Gram matrix $K \in \mathbb{R}^{N \times N}$ as $K_{ij} = \kappa(x_i, x_j)$. The normalized Gram matrix is defined as

$$A_{ij} = \frac{1}{N} \frac{K_{ij}}{\sqrt{K_{ii} K_{jj}}}. \quad (\text{A2})$$

Then, the matrix-based Renyi's α -order entropy is given by

$$S_\alpha(A) = \frac{1}{1-\alpha} \log_2 [\text{tr}(A^\alpha)] = \frac{1}{1-\alpha} \log_2 \left[\sum_{i=1}^N \lambda_i(A)^\alpha \right], \quad (\text{A3})$$

where $\lambda_i(A)$ denotes the i -th eigenvalue of A . The joint entropy can be defined as

$$S_\alpha(A, B) = S_\alpha \left(\frac{A \circ B}{\text{tr}(A \circ B)} \right), \quad (\text{A4})$$

where $A \circ B$ denotes the Hadamard product. From equations (A3) and (A4), the mutual information is defined as

$$I_\alpha(A, B) = S_\alpha(A) + S_\alpha(B) - S_\alpha(A, B). \quad (\text{A5})$$

The Gaussian kernel is commonly used:

$$\kappa_\sigma(x_i, x_j) = \exp\left(-\frac{\|x_i - x_j\|_F^2}{2\sigma^2}\right), \quad (\text{A6})$$

where $\|\cdot\|_F$ denotes the Frobenius norm. There are crucial factors that affect the estimation performance, such as the Gaussian kernel bandwidth σ and the scale and dimension of kernel input. The asymptotic behavior of entropy by varying σ can be denoted by

$$\lim_{\sigma \rightarrow 0} S_\alpha(A) = \log(N) \quad (\text{A7})$$

$$\lim_{\sigma \rightarrow \infty} S_\alpha(A) = 0. \quad (\text{A8})$$

Large scale and high-dimensional features of input give the same effect as small σ , which results in the overestimation of entropy. In contrast, small scale and low-dimensional features of input give the same effect as large σ , which results in the underestimation of entropy. Therefore, proper hyperparameter tuning is required for σ to avoid excessively large or small saturation of entropy during training. Scott's rule [29], a simplified version of Silverman's rule [30], is commonly used for selecting the width of Gaussian kernels:

$$\sigma = \gamma N^{-1/(4+d)}, \quad (\text{A9})$$

where γ is an empirically determined constant. Because equation (A9) is a monotonically increasing function with respect to feature dimension d , it compensates for higher feature dimension. We used $\gamma = 2$ for our experiments.

Saxe *et al.* observed that information estimation depends on the activation functions in a simple setup of a three neuron model ($x - z - y$) [9]. They sampled a scalar input x from a standard normal distribution of $\mathcal{N}(0, 1)$ and multiplied a constant weight w ; subsequently, they determined the hidden activity $z = f(wx)$ using a nonlinear activation function $f(s)$. Then, they discretized z and estimated the input mutual information $I(x; z)$ using a binning method. When the unbounded activation function of $f(s) = \text{ReLU}(s)$ was used, $I(x; z)$ continued to increase with w . However, when the bounded activation function of $f(s) = \tanh(s)$ was used, $I(x; z)$ first increased with w , and then decreased as w increased. This is a natural result when the binning method is used to estimate the mutual information because large activities are saturated with large w (figure 2 in [9]). We analyzed the same task with the kernel-based method (figure 5(a)). When the activation function is a sigmoid function of $f(s) = 1/(1 + \exp(-s))$, $I(x; z)$ does not decrease at large w ; however, the absolute value looks different from the unbounded activation functions of linear

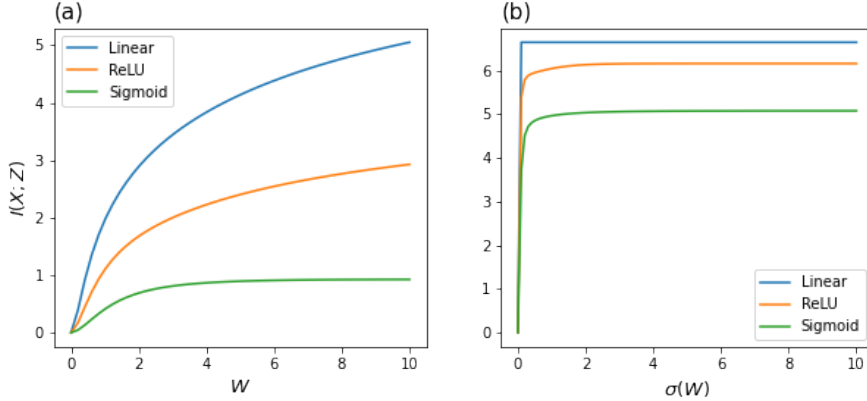


FIG. 5. Mutual information obtained by kernel-based estimation. (a) Input mutual information in a three-neuron network ($x - z - y$). Input x is sampled from a standard normal distribution and the hidden activity is computed by $z = f(wx)$, where w is the weight and $f(s)$ is an activation function. Three different activation functions (Linear, ReLU, and Sigmoid) are used. (b) Input mutual information for a general setup with 100-dimensional input vector X and 50-dimensional hidden vector $Z = f(WX)$. In this setup, weight W is a 50×100 matrix whose elements are sampled from a uniform distribution.

($f(s) = s$) and ReLU ($f(s) = \text{ReLU}(s)$). We also considered a more complex network with 100-dimensional input X sampled from $\mathcal{N}(0, 1)$. In this case, weight W was represented by a 50×100 matrix whose elements were sampled from a uniform distribution of $\mathcal{U}(0, 1)$; then, the hidden activity Z becomes a 50-dimensional vector, i.e., $Z = f(WX)$. We then observed $I(X; Z)$ while increasing the standard deviation of weight W (figure 5(b)). We confirmed that $I(X; Z)$ at large W does not decrease when a sigmoid activation function is used, like the unbounded activation functions of linear and ReLU. Therefore, this experiment demonstrated that the kernel-based method is a robust estimation technique for bounded activation function and the compression phase cannot be attributed to the selected activation function.

Appendix B: LAE: Label Autoencoder

LAE is a generative model that shapes its latent space using label classification. The explicit form of the LAE loss function is given as follows:

$$\mathcal{L}_{\text{LAE}} = \frac{1}{N} \sum_{i=1}^N \|X_i - X'_i\|^2 - \frac{\lambda}{N} \sum_{i=1}^N \sum_{j=1}^{n_Z} Y_{i,j} \log Z_{i,j}, \quad (\text{B1})$$

where N is the batch size and n_Z is the feature dimension of label. $Z_{i,j}$ is the softmax output of encoder that predicts the j -th class of the i -th sample and $Y_{i,j}$ is the corresponding true label. The first term is a reconstruction error (MSE) and the second term is a regularization given by the classification error of the encoder. The regularization coefficient λ is set to 0.01. Figure 6 shows the manifold learning of LAE when the one-hot vector corresponding to zero is changed to other digits as an input of the decoder. It is a two-dimensional submanifold embeded in a ten-dimensional label latent space.

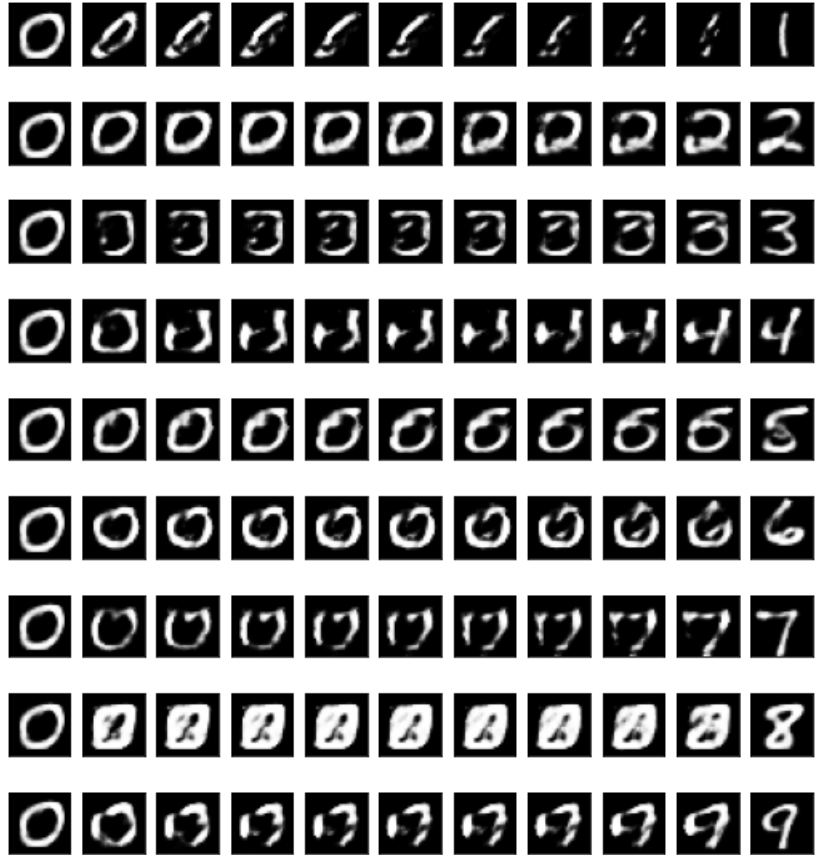


FIG. 6. Manifold learning in LAE. This represents the interpolation image when one-hot vector corresponding to zero, i.e., $Z_0 = [1, 0, 0, \dots, 0]$, is transformed to other digits as an input of the LAE decoder part. For instance, the first row represents the reproduction X' decoded from $Z = aZ_0 + (1 - a)Z_1$ by decreasing a from 1 to 0.